

Research



Cite this article: Alboussière T, Plunian F, Moulin M. 2022 Fury: an experimental dynamo with anisotropic electrical conductivity. *Proc. R. Soc. A* **478**: 20220374.
<https://doi.org/10.1098/rspa.2022.0374>

Received: 31 May 2022

Accepted: 9 November 2022

Subject Areas:

electromagnetism, astrophysics, geophysics

Keywords:

self-exciting dynamo, anisotropy, axisymmetry

Author for correspondence:

T. Alboussière

e-mail: thierry.alboussiere@ens-lyon.fr

Fury: an experimental dynamo with anisotropic electrical conductivity

T. Alboussière¹, F. Plunian² and M. Moulin³

¹Université Lyon 1, ENS de Lyon, CNRS, Laboratoire de Géologie de Lyon, Villeurbanne 69622, France

²Université Grenoble Alpes, Université Savoie Mont Blanc, CNRS, IRD, Université Gustave Eiffel, ISTERre, Grenoble 38000, France

³ENS de Lyon, CNRS, Laboratoire de Physique, Lyon 69364, France

TA, 0000-0002-3692-899X; FP, 0000-0002-4043-057X

We report measurements of dynamo action in a new experimental set-up, named Fury, based on the use of an anisotropic electrical conductivity. It consists of a copper rotor rotating inside a copper stator, electrically connected with a thin layer of liquid metal, galinstan. Grooves have been cut in the copper so that, everywhere, electrical conductivity can be considered to be that of copper along two directions while it is zero along the third one. The configuration is efficient and dynamo action can be powered by hand. We have also used a motor with better control, enabling us to drive the rotor at specified velocity or torque functions of time. The structure of the axisymmetric magnetic field produced is found to be close to the numerical modelling using FreeFem++. The experimental dynamo behaves very nearly as expected for a kinematic dynamo, so that the threshold dynamo velocity cannot be exceeded, or only briefly. More mechanical power in the rotor rotation leads to an increase in the magnetic field intensity, the magnetic energy being proportional to the extra mechanical power beyond the threshold. In the transient following a step increase of torque, magnetic and angular velocity oscillations have been observed and explained.

1. Previous dynamos

The notion ‘dynamo’ can refer to different machines and was historically used to designate a device transforming mechanical energy into continuous electric current.

Faraday's dynamo was the first [1]: a disk rotating in the magnetic field generated by a permanent magnet leads to an electric potential difference between its centre and rim and to an electric current when they are connected. This fundamental discovery—induction—was then used in more powerful machines to produce electricity from mechanical energy (the names of Pixii in France, Pacinotti in Italia, Woolrich in England are associated with such machines). However, they needed many heavy magnets to produce a modest electric power. This was at the origin of the concept of 'self-exciting dynamos'. The idea was to reinforce (or excite) the magnetic field of the permanent magnets by diverting a fraction of the electric current produced by the machine and wind it around the magnets, thus becoming electro-magnets. Ányos Jedlik, around 1856 in Győr in the kingdom of Hungary (at the time), seems to have been the first inventor of such a machine, but his work remained unknown for a long time. He was followed by Hjorth in Denmark, Siemens in Germany, Gramme in France, Wheatstone & Wilde [2] in England. Note, however, that the self-exciting dynamos needed some residual magnetization in their iron parts when they were started: initially the motion of the rotor in the residual magnetic field produces a small electric current that is used to feed the electromagnets, so that the same rotation rate produces more current up to the point when part of it can be used to power an external load. This is so true that a well-known cause of failure is the lack of residual magnetism sometimes due to a long period of inactivity. In such a case, the dynamo will not produce electricity even at high rotor speed and the solution known as 'flashing the field' consists in having an external generator, or a battery, discharge electricity in the windings of the electromagnets to restore residual magnetism. Even now, this solution can be found on the web when a car alternator does not work. Another hint of the importance of residual magnetization comes from visits to electricity museums: even after many decades of inactivity, all these self-exciting dynamos have a magnetic field of several hundreds of Gauss, as can be measured by anyone with a smartphone and the excellent application PhyPhox [3] giving access to all sensors (acceleration, sound, pressure, magnetic field) present in these mobile devices.

Here, by 'dynamo', we mean a device or a natural object producing a magnetic field from the motion of electrically conducting materials, in the absence of magnetized materials (or materials with magnetic properties in the strictest acceptance). Many planets and all stars have a self-generated magnetic field, whereas their internal temperature is above the Curie point, precluding any magnetic effect. In this context, the corresponding concept of self-exciting dynamo of Bullard [4] differs definitely from the historical definition mentioned above. Self-excitation now refers primarily to the capacity of the dynamo to operate in the absence of any initial magnetic field. We expect—and this is true for Bullard dynamos—that an instability threshold is reached when the rotation rate is large enough, above which the magnetic field and electric current will jointly grow simultaneously exponentially (initially). This corresponds to a supercritical bifurcation, which is the case in most self-exciting dynamo models in the modern geophysical and astrophysical sense. By contrast, we formulate the hypothesis that the historical self-exciting dynamo machines of the nineteenth century were probably dynamos in a subcritical regime, with an instability threshold above the usual range of nominal rotation rates. Alternatively, their different behaviour could be due to the nonlinearities: a residual (remanent) magnetic field is a positive nonlinearity when it is present, however contact resistance at sliprings constitutes a very negative nonlinearity for dynamo action. Magnetic saturation is also a nonlinear effect but should not impact the starting phase of dynamos.

Concerning modern experimental realizations of self-exciting dynamos, with solid or liquid electrical conductors, there have been four self-generated experimental dynamos published in the literature. One is a 'solid' dynamo [5,6], the other three have used liquid sodium [7–9]. Soon after the first theoretical dynamo model [10], Lowes & Wilkinson [5] made an experimental version of it, consisting of two cylindrical electrically conducting rotors, rotating in cylindrical bores in a solid sphere (or a cube in the second version) and in electrical contact through a film of liquid metal (mercury). Both rotors and the sphere have been made of soft iron to increase the magnetic permeability by a factor of 250 (150 in the second version), in order to lower the dynamo threshold in terms of angular velocities. Dynamo action was reached with approximately

200 W of mechanical energy. It took time and effort before fluid dynamos were realized. In 2000, experiments in Riga [7] and Karlsruhe [8] showed that dynamo action was possible with liquid sodium. In Riga, a flow inspired from the Ponomarenko model [11] was set up: a turbine propelled the fluid with strong rotation in a pipe, the fluid was then channelled back around the pipe while its rotation was stopped using baffles [7]. Dynamo action was obtained with 100 kW and 1.5 cubic metres of sodium. In Karlsruhe, an arrangement of helical pipes produced an array of helical flows of the same helicity sign. This is an approximation of the G.O. Robert's model [12]. With 1.6 m³ of sodium and about 500 kW, a stationary magnetic field was produced [8]. Finally, in Cadarache, the VKS experiment produced a dynamo effect in a cylinder with two counter-rotating discs at each end [9]. This arrangement can be seen as a realization of a Taylor-green vortex, although the flow becomes highly unsteady and turbulent for a moderate rotation rate of the discs. The discs had to be made of iron in order to reach the dynamo threshold. This set-up required 160 l of sodium and 150 kW for dynamo action.

With the more restrictive definition excluding magnetic properties, only two of the four experiments are dynamos: Riga and Karlsruhe dynamos. Their mean flow is well constrained and their dynamo threshold was predicted correctly from the kinematic dynamo analyses. Of course, above the threshold, the flow was altered by the magnetic field and a non linear dynamo regime was observed [13,14], involving a change in the structure of the flows. On the contrary, the Cadarache dynamo is less constrained in terms of flow structure. The dynamo threshold was not predicted from the mean flow and a larger variety of nonlinear behaviours have been observed [15]. In all three cases, the mechanism of saturation above the threshold is not completely understood [7,16,17]. This is partly due to the fact that the set-ups have a limited amount of mechanical power and cannot reach velocities much above threshold, and partly due to the difficulty in detecting very subtle changes in the velocity field.

2. Fury: from copper and grooves

From our previous theoretical investigations on anisotropic electrical conductivity [18,19], we know that a dynamo can have a planar velocity field and/or produce an axisymmetric magnetic field. We have built an experimental setup which is a rotor inside a stator (figure 1). The final external diameter of the stator is 170 mm, its length is 209 mm and its internal diameter is 101 mm. The rotor that fits inside has the same length and an external diameter of 100 mm, hence the gap between rotor and stator is 0.5 mm wide. It has an internal diameter of 30 mm so that a (non-magnetic) steel axis can be fitted in. The grade of copper for rotor and stator is CUA1 H12, with a guaranteed electrical conductivity σ between 100 and 102.5% IACS, i.e. $\sigma = 5.8 \cdot 10^7 \Omega^{-1} \text{ m}^{-1}$ to $\sigma = 5.95 \cdot 10^7 \Omega^{-1} \text{ m}^{-1}$.

Grooves have been cut in the rotor and stator, extending across the whole length and forming arcs of logarithmic spirals in the perpendicular cross-section: the direction along the groove makes an angle of 62° with the radial direction at all points. In the stator 35 equally spaced spirals have been cut and 20 in the rotor. The grooves have been cut with the technique of electro-erosion, with each groove having a width of 0.33 mm. The grooves have then been filled with a polyimide film and epoxy resin for electric insulation and mechanical strength. As can be seen on the left-hand side of figure 1, the internal diameter of the stator was cut 20 mm smaller initially to ensure rigidity during the cutting of the grooves (similarly, the external diameter of the rotor was larger by 20 mm). After the epoxy resin hardened, the stator internal and rotor external diameters were cut to the final dimensions, leaving a radial distance of 2 mm to the end of the grooves. This ensures a good precision and small roughness of the surfaces involved in the differential rotation. These surfaces (external of the rotor and internal of the stator) were then silver plated (a few micrometres) for chemical protection of the copper and to ensure good electrical contact with galinstan.

The assembly of the setup is quite simple, with two flanges at the top and bottom tied with threaded rods, ensuring mechanical cohesion with ball bearings inserted to hold the axis of the rotor. The 0.5 mm gap between rotor and stator was filled with galinstan, an alloy of gallium,

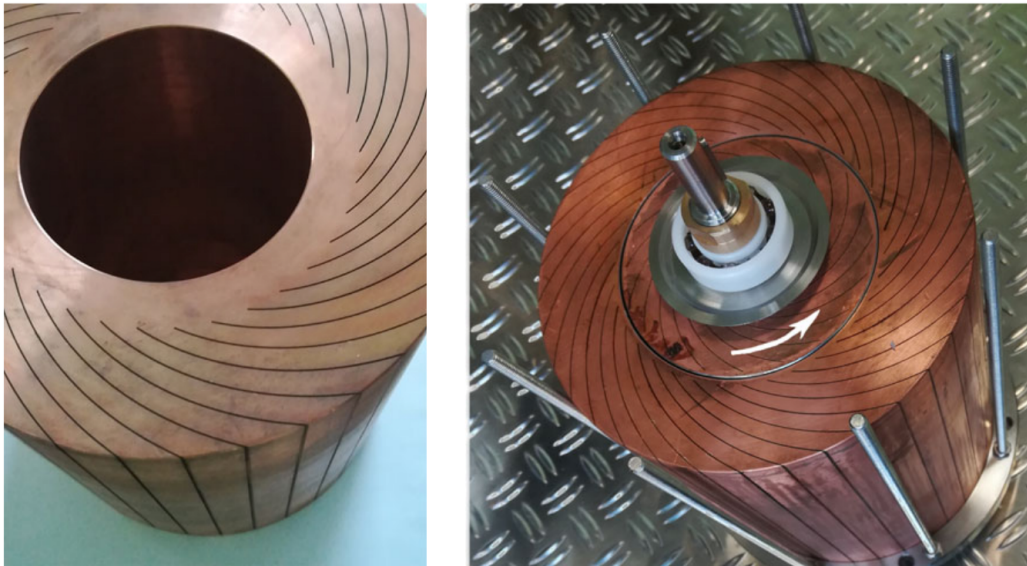


Figure 1. Grooves are cut in a copper rotor and stator. (Online version in colour.)

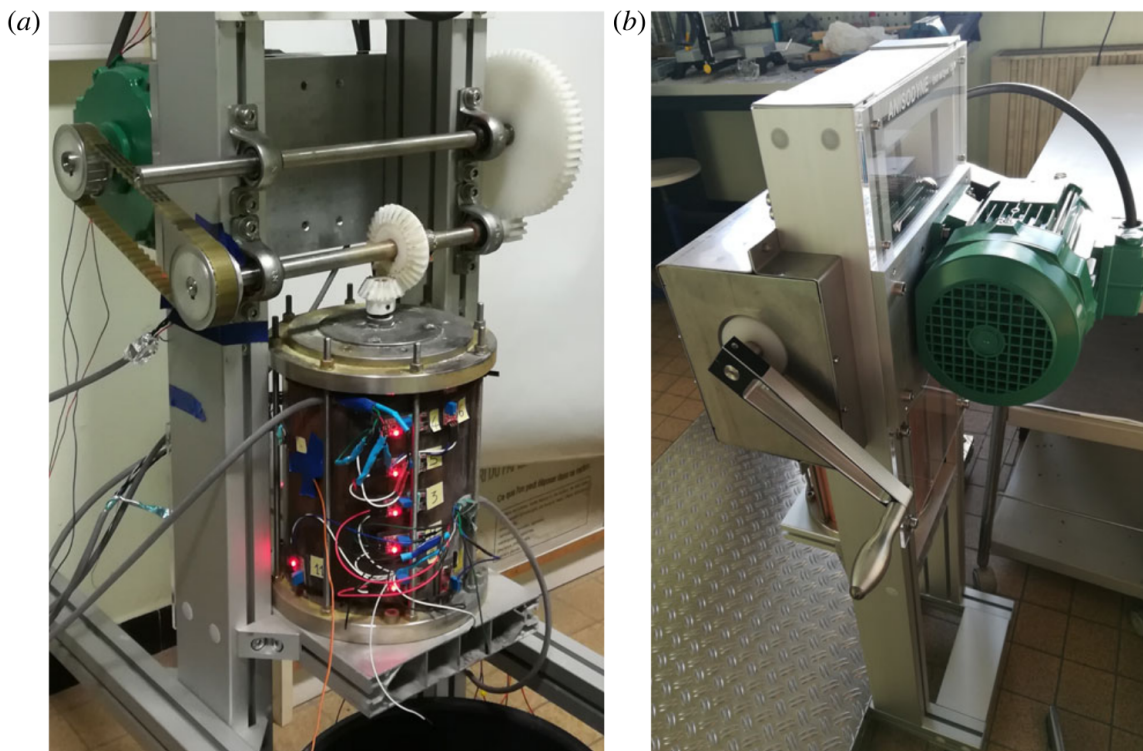


Figure 2. Front view of Fury (a) and side view (b). (Online version in colour.)

indium and tin, liquid at room temperature. In figure 2 showing the final setup, the copper stator is still visible and the rotor axis is connected through gears and belt to a handle and to an electric motor. Manual or motor operations are possible. One turn of the handle (resp. electric motor) corresponds to 12 (resp. 2) turns of the rotor axis.

Measurements are made of the magnetic field from Hall probes on the external surface of the stator: each Hall probe has a small red LED (figure 2). The electric variator of the motor provides measurement of angular velocity and torque.

3. Fury: dynamo results

The dual operation, manual or motor-powered, has two distinct objectives. Powering the experiment by hand is interesting, giving a direct physical feeling of dynamo action: one can feel the mechanical resistance due to Lorentz forces when the magnetic field is generated. However,

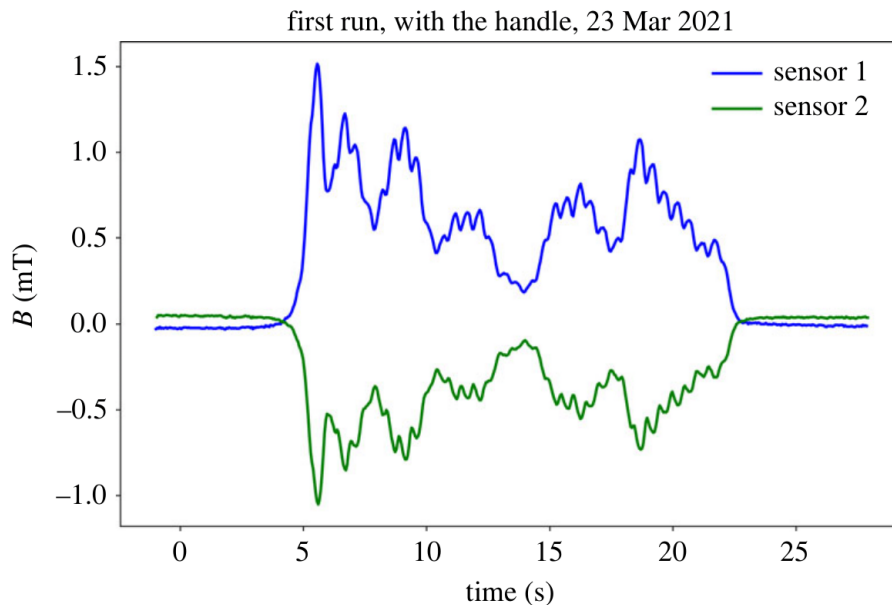


Figure 3. First dynamo action with Fury, human-powered with the handle. (Online version in colour.)

the conditions of operation are not well controlled: neither the velocity nor the torque are constant and both are operator-dependent. Using a motor brings the possibility to follow almost any prescribed function of velocity or torque, within the limit of its maximal power.

(a) The first successful human-powered dynamo run

The very first run of dynamo action with Fury took place on 23 March 2021. In figure 3, one can see the signal of the two Hall probes (at the time) stuck on the outside of the stator. Those two signals are proportional to each other, although the two probes were at different places and had different orientations. This hints at the fact that the self-generated magnetic field is made of a single mode. Only its magnitude can change with time. Let us analyse the time evolution of this run. The operator ran the handle until it reached about 2 Hz, at a time between $t = 2$ s and $t = 3$ s. The magnetic field started to depart from its initial value (the ambient magnetic field). At a time of nearly $t = 6$ s, it peaked to a maximum. At the same time, the operator had experienced an extra resistance from the Lorentz forces, which led to a decrease in the rotation rate and irregular decay of the magnitude of the magnetic field. At $t = 13$ s, the operator recovered a little and put more effort in for a while, then stopped at $t = 22$ s or so.

Another piece of information from the signals in figure 3 is the presence of a 2 Hz oscillation. This is precisely the frequency of the handle rotation. The interpretation is that the input of energy is not constant over one rotation of the handle, which seems quite plausible. Note that the ratio between handle and rotor rotation is 12 (a factor 6 in the gears between the horizontal axes, see figure 2, and 2 in the conical gears on top of the rotor). This implies that the threshold for dynamo action corresponds to an angular velocity around 24 Hz for the rotor.

As will be seen later, reaching 2 Hz with the handle requires an input of 230 W of mechanical work to overcome the resistance of the galinstan film (main contribution), ball bearings and gears. This is quite an effort with a handle, but all operators over a representative sample of ten colleagues (two women, eight men) could do it. The good news is that the effort does not need to be sustained for a long time. Within 5 s, it is usually possible to start the dynamo.

(b) More results with a motor

Most results have been obtained with an electric motor of maximal power 750 W (about one horse power). This is just a little bit more than what the average human can do, but it can sustain it for longer and can adjust the effort very precisely.

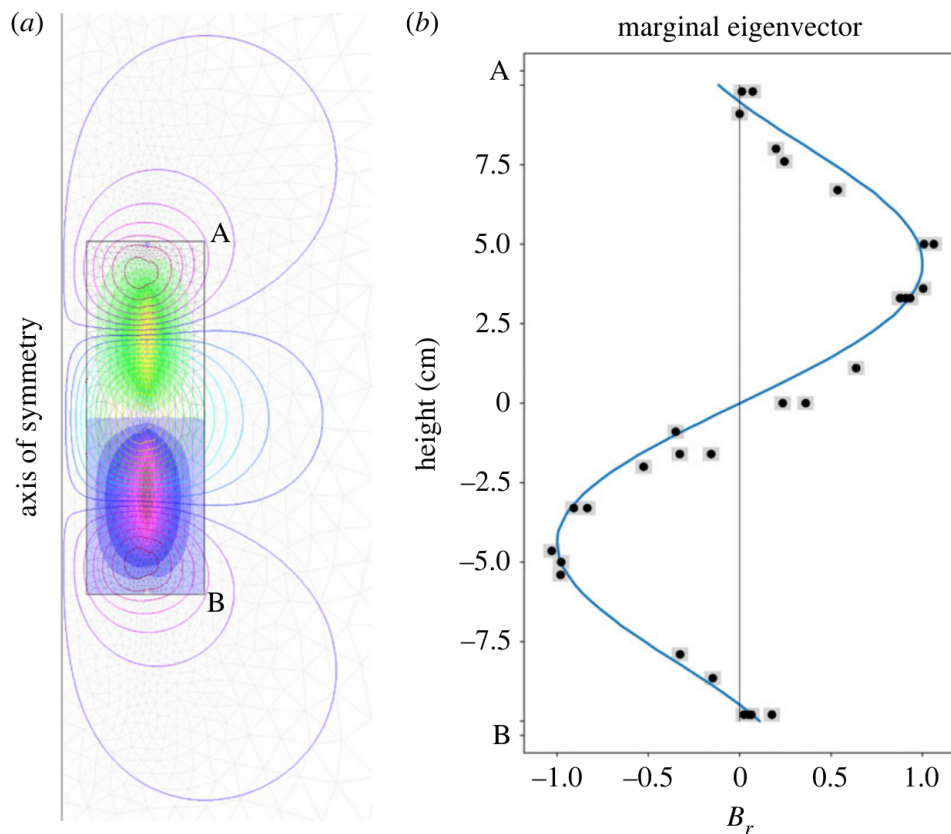


Figure 4. Eigenmode at marginal stability from finite element modelling (FreeFem++) on (a), profile of B_r (FreeFem++ and measured on Fury) on (b). (Online version in colour.)

(i) Marginal eigenvector

Using FreeFem++ [20], we have built a numerical Fury model. This model is assumed to be axisymmetrical as the magnetic field observed in the experiment is itself axisymmetric. Electrical conductivity is taken to be anisotropic in the copper parts. This means that we have not attempted to model each copper blade, but have used a mesoscale anisotropic modelling instead. The finite-element model takes into account the thin galinstan gap with its isotropic electrical conductivity about 16.8 times smaller than that of copper. The induction equation is considered, with a solid rotation of the rotor, and a linear profile in the galinstan gap to reach a zero velocity in the stator. Outside the conducting domain, the magnetic field obeys a harmonic equation.

We have computed the marginal eigenvalue and eigenvector at the lowest possible rotation rate. This (axisymmetric) eigenmode is shown in figure 4: the mesh used for the finite-element calculations is shown in the background, the toroidal isovalues are shown with colour level in the rectangular conducting domain (rotor-galinstan-stator) and some field lines of the poloidal component are drawn. Figure 4b, the cylindrical radial component of the magnetic field, is plotted along the profile A–B on the outside surface of the stator (blue curve). The black dots are measurements of the same Fury profile. The grey region around each point corresponds to the uncertainty of position (± 2 mm and magnetic field $\pm 5\%$ of the maximum value, mainly due to orientation errors of Hall sensors). These points correspond to different runs and to different azimuthal angles. Considering the accuracy of the measurements, there is no sign of departure from axisymmetry. The agreement between the calculated profile and the measurements is quite good: it seems that the experimental values are slightly shifted to the bottom compared with the calculated odd profile.

Let us now consider the value of the magnetic Reynolds number corresponding to marginal stability. Let us define the magnetic Reynolds number as $Rm = \mu\sigma UR$, with σ the electrical conductivity of copper, $\mu = 4\pi \times 10^{-7} \text{ H m}^{-1}$ the magnetic permeability of copper (or of vacuum), $R = 0.05$ m the radius of the rotor and $U = \omega R$ the maximal tangential velocity of the rotor (ω is

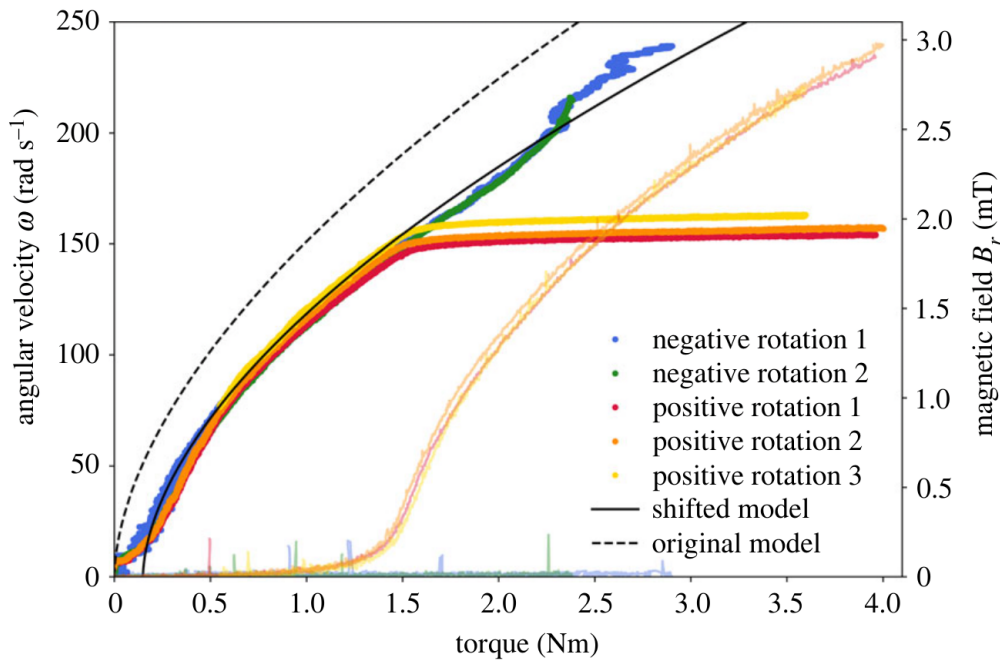


Figure 5. Angular velocity (bright colours) and magnetic field (faded colours) versus torque, for two runs in the negative direction and three runs in the positive (dynamo) direction. (Online version in colour.)

the angular velocity). A rotation rate of the rotor of 24 Hz corresponds to an angular velocity of 150 rad s^{-1} . However, with the motor and more precise velocity measurements, we could get dynamo action for $\omega \simeq 147 \text{ rad s}^{-1}$ (red curve in figure 5). This leads to a critical magnetic Reynolds number of $Rm_c \simeq 26.8$. The dynamo threshold obtained with FreeFem++ is $Rm_c \simeq 23.1$. The difference can be explained firstly by the presence of a finite number of discrete grooves in the experiment, compared to a uniform anisotropy in FreeFem++ calculations. Secondly, the grooves correspond to a removal of about 5% of the total mass of copper. This would already explain an increase by 5% of the threshold. There can also be a contact electrical resistance between the copper and the film of galinstan. For completeness, the analytical threshold is $Rm_c \simeq 14.61$ with an infinitely long configuration and a stator of infinite radius (and in the absence of a layer liquid galinstan of electrical conductivity 16.8 times smaller than that of copper) [19].

In accordance with theoretical investigations [18,19], when the imposed rotation has the opposite direction, dynamo action never happens: all eigenvalues from FreeFem++ have a negative real part. Similarly, no dynamo action can be seen in Fury with the negative rotation.

(ii) Torque, power and magnetic energy

Increasing linearly the imposed torque from zero to its maximum value, we have been able to plot the resulting curves in the diagram shown in figure 5. Three runs in the ‘positive’ direction of rotation are shown, and two in the reverse ‘negative’ direction (see figure 1 where the white arrow defines positive rotation). In agreement with the mathematical analysis [18,19], dynamo action is possible only with the positive direction of rotation. At low rotation rate, below the dynamo threshold, all curves follow the same path. The relationship between the angular velocity and the torque is determined by hydrodynamical properties of the galinstan alloy with additional torque contributions from the ball bearings (outside on the visible axes on figure 2, inside to support the axis of the rotor as shown in figure 1) and gears. The dashed black curve (original model) in figure 5 corresponds to the turbulent model by Orlandi *et al.* [21].¹ Note that at a typical rotation rate of 24 Hz, the Reynolds number of the galinstan in the gap is approximately 5000 (plane

¹A fit for the friction coefficient c_f is proposed for the turbulent Couette flow in terms of the Reynolds number Re , based on various experimental results $c_f = 0.056 Re^{1/4}$. The Reynolds number is $Re = Uh/\nu$, where U is half the velocity difference across a layer of thickness h of a fluid of kinematic viscosity ν . The resulting shear stress is $\tau_w = \frac{1}{2} c_f \rho U^2$ by definition of the friction coefficient c_f .

Couette flow is generally turbulent above Reynolds number 10^3). The continuous black curve (shifted model) is derived from the first one with a multiplication by 1.3 and with the addition of a constant resistive torque of 0.15 Nm, for a best fit of the data. No attempt was made to measure the fluctuations of the torque (for an imposed velocity) or of the velocity (for an imposed torque) that would be due to hydrodynamic turbulence in the gap of galinstan. We expect those fluctuations to produce a small average effect (over the whole gap) and to be impossible to measure from the variator of the electric motor.

In the positive direction of rotation, above 150 rad s^{-1} , further increasing the torque does not result in an increase in angular velocity. The self-generated dynamo behaves pretty well like a kinematic dynamo: it is virtually impossible to exceed the threshold angular velocity (150 rad s^{-1} corresponds to $150/(2\pi) \simeq 24 \text{ Hz}$). Increasing the torque leads to an increase in the self-generated magnetic field (fade colored curves in figure 5). On the contrary, in the negative direction of rotation, the same 'hydrodynamical' curve is followed as for lower velocities and no magnetic field is generated.

In the dynamo regime (positive direction), a careful examination reveals that the angular velocity increases very slightly when the torque is increased above the threshold. However, most of this increase is due to the effect of temperature. As the system dissipates energy (by turbulence and viscosity at small scale, by Joule heating when the dynamo is running) the copper of the rotor and stator gets heated, hence its electrical conductivity decreases. In order to maintain the kinematic dynamo at its critical magnetic Reynolds number, a decrease in electrical conductivity has to be compensated by a similar relative increase in angular velocity. In figure 5, the three dynamo runs, 1 to 3, were obtained while the temperature of the outside surface of the stator was 20.2°C , 22.4°C and 25.6°C , respectively. With a linear thermal coefficient of $4.3 \cdot 10^{-3} \text{ K}^{-1}$ for copper, the difference in temperature of 5.4 K leads to a relative variation of 2.3% in electrical conductivity. The relative difference in angular velocity between run 1 and run 3 is about 5%. We do not have a definite explanation for this mismatch: one possibility is that the temperature difference in the interior of the setup was larger than that measured on the external surface.

Anticipating on the next §3b(iii), we can see in figure 7 that the magnetic energy grows linearly with the input mechanical power injected in the setup, when the dynamo threshold is exceeded. In that regime, any extra power input is dissipated by an extra Joule dissipation. This is coherent from the point of view of magnetohydrodynamics, as Joule dissipation scales usually proportionally to the square of the magnetic field for a given velocity field, in the magnetic diffusive regime.

(iii) Torque steps, torsional oscillations

When the experimental setup Fury is run with an electric motor, we can impose a torque and step changes over a very short duration of less than 0.1 s. In figure 6, we show the time evolution of an experiment where we have imposed 12 steps of increasing torque (labelled 1–12) and the reverse 12 steps of decreasing torque, in a black continuous line. Each step duration is 10 s and the maximum torque was 4 Nm. As a result of these torque changes, angular velocity (blue line) increases significantly for the first 5 steps, then remains globally at the same level and finally goes down in the last 5 steps. After step 5 and until just before step 20, self-exciting dynamo is at work, as shown by the value of the magnetic field (red curve), which maintains the angular velocity close to the dynamo threshold. The dynamo has actually perhaps started after the 4th step, as we can see a low level of magnetic field already. This is an indication that the dynamo threshold is not as sharp as expected for a kinematic dynamo, within a range of angular velocities, and we shall later explore this phenomenon.

In figure 7, the same experiment is represented in terms of mechanical energy input from the motor and square of the magnetic component B_r on the external surface of the stator (position $z = 3.7 \text{ cm}$ along the profile A-B in figure 4). In this diagram, the time evolution of the run is plotted in red while the torque is increased, then in blue for the second part of decreasing torque. In the dynamo regime, each step increase of the torque leads to an increase of mechanical power,

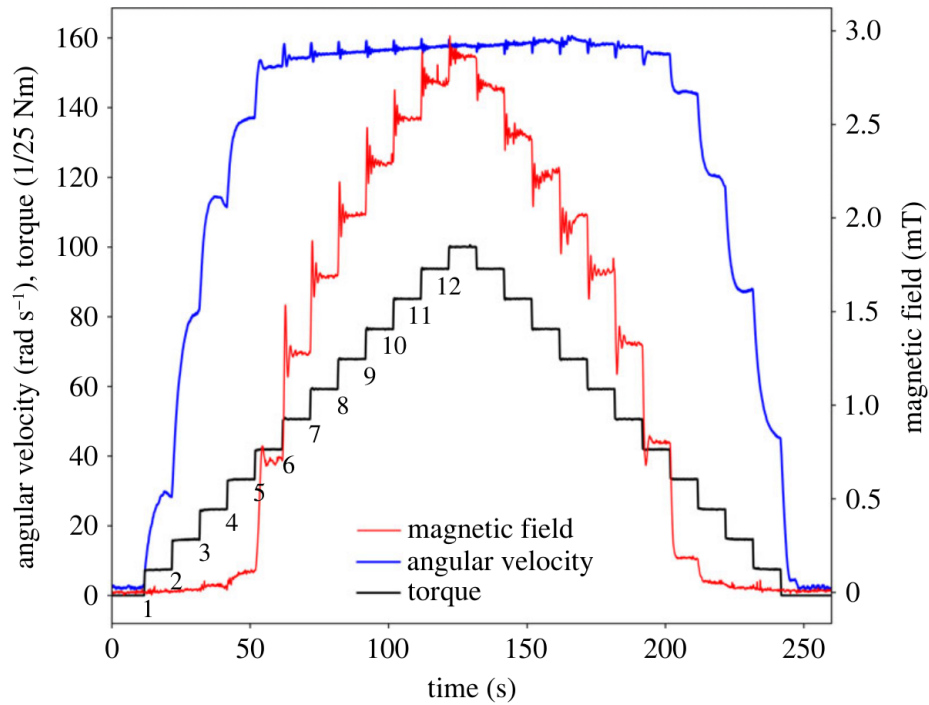


Figure 6. Angular velocity, torque, magnetic field in a single run with imposed steps of torque in the positive direction of rotation. (Online version in colour.)

followed by an increase of the magnetic energy. There is a transient phase of oscillations towards a final stationary regime where the path follows a converging spiral. The oscillations of the magnetic field can also be seen in figure 6 after each torque step. When the torque steps are in the decreasing phase (blue line), we observe a similar trend: the mechanical power goes down quickly and a phase of oscillating magnetic field follows with a final lower level of magnetic field. As mentioned above, the stationary points are well aligned along a straight line and we find a good agreement with the expression $B_r^2 = 0.0204(\mathcal{P} - 231)$ above the dynamo threshold (B_r in mT and the mechanical power input \mathcal{P} in Watt).

In figure 6, it seems that the oscillations get faster as the magnetic field increases. We plot the oscillations following steps 5–12 in figure 8, using a dimensionless timescale proportional to the intensity of the magnetic field. Specifically, we use a timescale relevant to Alfvén waves, $tB_r/(R\sqrt{\rho\mu})$ with $R = 0.05$ m the radius of the rotor, $\rho = 8960$ kg m⁻³ copper density, $\mu = 4\pi \cdot 10^{-7}$ H m⁻¹ magnetic permeability and B_r (in Tesla) the limit radial magnetic field after each step. The oscillations of B_r superimpose nicely in this dimensionless timescale, and their period is of order one (close to 0.5). In the inset of figure 8, we have plotted again the magnetic signal after one of the steps (step 9), along with the signal of angular velocity fluctuations. Those signals are in phase quadrature relative to each other, similarly to Alfvén waves [22]. Because of the axisymmetry of the configuration and magnetic mode, these oscillations seem to be of the same nature as a particular kind of Alfvén wave, i.e. torsional oscillations. Such oscillations have been detected in the Earth’s core [23] from geomagnetic data and also in an experiment with liquid sodium [24].

However, they are not Alfvén waves, nor associated torsional oscillations. Alfvén waves develop when kinematic and magnetic diffusion are negligible. Here, even with the highest magnetic field, the period of the oscillations is just under one second, while magnetic diffusion through 5 cm of copper is about 0.02 s. The oscillations are related to the dynamo mechanism itself: after a step, the system is pushed initially in the supercritical domain $Rm > Rm_c$, leading to a positive growth rate of the (global diffusive) magnetic field. The resulting increase of dissipative Lorentz forces brings the velocity down and the setup enters the subcritical domain $Rm < Rm_c$ with a deficit in Lorentz forces compared to the applied torque. The rotation increases and this is

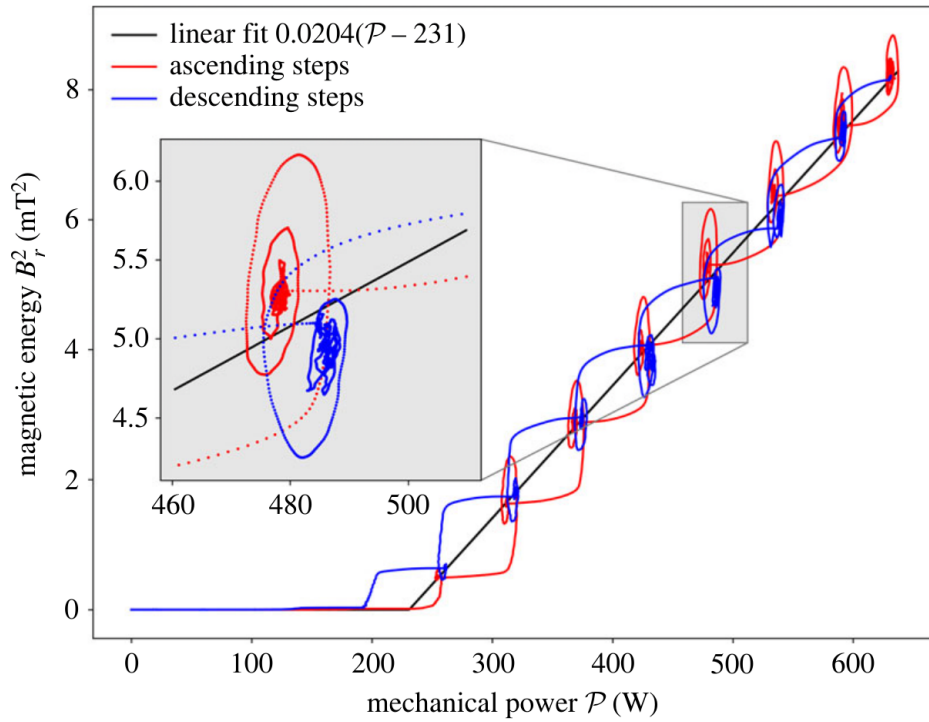


Figure 7. Square of the measured magnetic field B_r^2 as a function of the mechanical power input \mathcal{P} during the run shown in figure 6. (Online version in colour.)

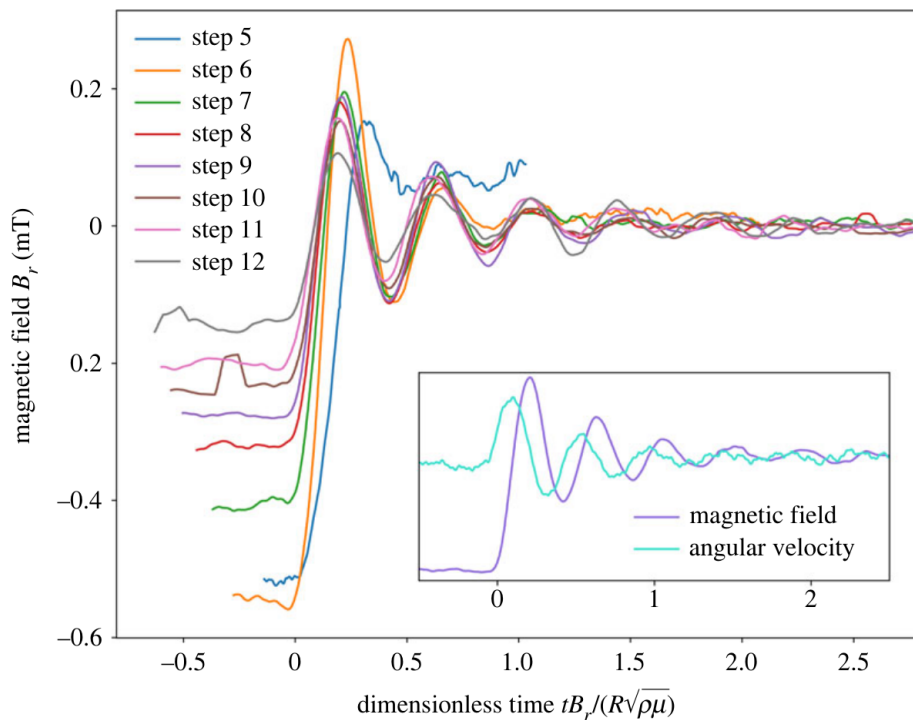


Figure 8. Stack of magnetic field oscillations after steps of torque (see figure 6 for the numbering of steps) with the dimensionless time scale $tB_r/(R\sqrt{\rho\mu})$. The inset (step 9) shows that the corresponding oscillations of angular velocity are in phase quadrature relative to magnetic oscillations. (Online version in colour.)

the start of a new period of the oscillations. The dynamic equation for the rotor rotation ω can be written approximately as follows:

$$\rho R^2 \frac{d\omega}{dt} \simeq -\sigma \omega R^2 B_r^2 - T_v + T, \quad (3.1)$$

where $-\sigma\omega R^2 B_r^2$ is the Lorentz torque, $-\mathcal{T}_v$ the viscous torque and \mathcal{T} the constant torque provided by the motor, per unit volume. Assuming the viscous torque to be constant, taking the time derivative leads to

$$\rho R^2 \frac{d^2\omega}{dt^2} \simeq -2\sigma\omega R^2 B_r \frac{dB_r}{dt} - \sigma R^2 B_r^2 \frac{d\omega}{dt}. \quad (3.2)$$

From our previous studies of the anisotropic dynamo, see eqn (C17) of [18] and (4.18) of [25], we know that the growth rate of the magnetic field is proportional to $\omega - \omega_0$ (with a constant of order unity) near the dynamo threshold ω_0 for angular velocity. Substituting $dB_r/dt = (\omega - \omega_0)B_r$ in equation (3.2) and dividing by ρR^2 , one obtains

$$\frac{d^2(\omega - \omega_0)}{dt^2} \simeq -2\frac{\sigma B_r^2}{\rho}\omega_0(\omega - \omega_0) - \frac{\sigma B_r^2}{\rho} \frac{d(\omega - \omega_0)}{dt}. \quad (3.3)$$

The last term on the right-hand side is negligible provided the timescale of the solution is longer than ω_0^{-1} . Making this assumption leads to a simple harmonic equation, of associated timescale $\tau = \sqrt{\rho/(\sigma\omega_0 B_r^2)}$, which is the geometric average of the (short) turnover timescale ω_0^{-1} and the (long) Joule damping time $\rho/(\sigma B_r^2)$. It is longer than ω_0^{-1} , hence our assumption is justified: it is also coherent with the smaller relative oscillations of angular velocity compared with those of the magnetic field in figure 6 after each step. This timescale τ can be expressed using $Rm_c = \mu\sigma\omega_0 R^2$ under the form

$$\tau = \frac{1}{\sqrt{Rm_c}} \frac{R}{V_A}, \quad (3.4)$$

where $V_A = B_r/\sqrt{\rho\mu}$ is the Alfvén velocity. This timescale τ is the timescale we have used to plot figure 8, without the constant $1/\sqrt{Rm_c} \simeq 1/5$. Even though the physics is different from that of Alfvén waves, a similar timescale arises from the coupling between rotor inertia and dynamo growth rate.

4. Nature of the bifurcation

We plot in the same figure 9 different results concerning the dynamo bifurcation, as the measured magnetic field as a function of the torque imposed. This only concerns the ‘dynamo’ direction of rotation, since no magnetic field is generated in the other direction as expected from the theory. We replot the magnetic curves shown in figure 5, obtained with a (slow) continuous increase of the imposed torque. Then we also plot the steady value of the magnetic field reached after the transient period following each torque step shown in figure 6. We observe that all measurements (continuous or steady) fall on a similar curve depicting an imperfect supercritical bifurcation, starting at a torque value of 1.5 Nm with an exponent close to 1/2 for the magnetic field. This bifurcation diagram is coherent with the evolution of magnetic energy as a function of mechanical power shown in figure 7, considering that the velocity remains constant near 150 rad s⁻¹ above the dynamo threshold.

No clear hysteresis has been observed: increasing and decreasing steps of torque lead to points falling on the same curve. This applies also to the imperfect part of the bifurcation. Possible reasons for the imperfection could be related to the Earth ambient magnetic field, or to small magnetic metallic pieces (bolts, ball bearings, gears) that have not been eliminated completely. Another observation is probably associated with the imperfect bifurcation: the magnetic field produced always has the same orientation, whereas the opposite orientation should be as likely. The imperfect bifurcation is thought to drive the eigenmode in a definite orientation, not random.

Concerning the critical exponent 1/2 of the increase of the magnetic field above the critical torque threshold, it is directly related to the fate of the mechanical energy dissipated in the system, as discussed previously. This dynamo behaves very closely to a kinematic dynamo: the solid parts possess no freedom to deform and change the induced magnetic field, whereas the liquid part is restricted to a very narrow gap of 0.5 mm so that, even if changes occur they will have a very limited impact. This implies that the velocity does not change above the critical

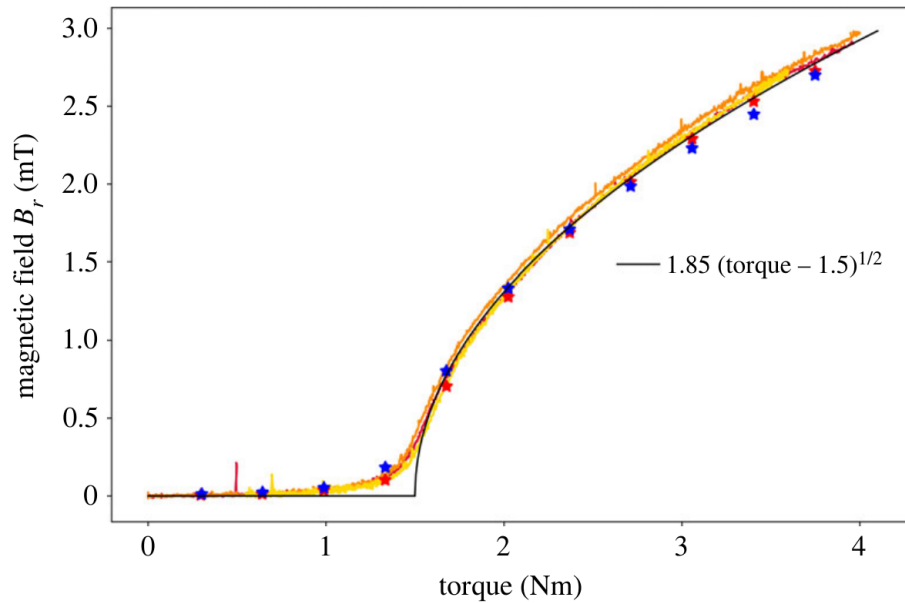


Figure 9. Measured magnetic field B_r as a function of the torque input. The continuous coloured lines correspond to continuous variations of the torque shown in figure 5 and the stars to the imposed torque steps shown in figure 6, red (resp. blue) stars corresponding to increasing (resp. decreasing) torque steps. (Online version in colour.)

torque. Hence (turbulent) dissipation remains constant in the liquid gap.² The extra mechanical power injected above the threshold is entirely dissipated as Joule dissipation. As the form of the magnetic field remains the same, the magnetic field is proportional to the electric currents, which are proportional to the square root of Joule dissipation. With a nearly constant velocity, mechanical power is proportional to the torque, which explains why the magnetic field intensity grows like the square-root of the torque above threshold.

On the contrary, in Karlsruhe, Riga and Cadarache dynamos, the mean velocity of the flow can be increased above the threshold value for dynamo action. Also, the extra power above threshold goes mostly into hydrodynamical turbulent dissipation while a smaller part is dissipated through the Joule effect. There have been arguments to suggest a scaling such as $B^2 \sim V - V_c$ [13,27], where B is the magnetic field, V the mean velocity and V_c the dynamo threshold velocity. These arguments can be based on dimensional analysis or on the scaling of the Lorentz forces on the mean flow. Combined with a turbulent dissipative scaling $\mathcal{P} \sim V^3$ for the required mechanical power \mathcal{P} , the resulting scaling for the magnetic field is $B \sim \sqrt{\mathcal{P}^{1/3} - V_c}$ which can look like anything between $\mathcal{P}^{1/2}$ and $\mathcal{P}^{1/6}$ depending on the proximity to the threshold.

Let us now compare the dynamo bifurcation observed in Fury to that observed in the Lowes and Wilkinson dynamo. Both dynamos require a similar power of the order of 200 W, but the dynamo of Lowes and Wilkinson had to be made in a magnetic material so that its dynamo threshold could be reached. In their first paper [5], Lowes and Wilkinson show that they could increase the velocity of one of the cylinders above the critical velocity and that this led to an increase of the magnetic field intensity. This is different in Fury where the velocity cannot be made larger than the threshold velocity as the magnetic field would grow indefinitely in amplitude. In their second paper [6], Lowes and Wilkinson observe oscillations of the magnetic field (and of the rotation rates of the cylinders) above dynamo threshold. Such oscillatory regimes have been found in more recent numerical simulations of the Herzenberg dynamo [28], but they could only be seen at a much larger magnetic Reynolds number. Lowes and Wilkinson admit that the magnetic material (saturation and remanence) might play a large role in the observed regimes.

²Turbulent friction (and dissipation) in the galinstan layer is not affected by the magnetic field unless $c_f Re^2 / Ha^4 < 1$ according to Alboussière & Lingwood [26]. This would require the Hartmann number $Ha = \sqrt{\sigma / (\rho\nu)} Bh$ to be more than 100 times larger than it is estimated with a magnetic field of 3 mT.

Their last sentence expresses their regrets that they had to use a magnetic material: ‘We hope by further improvement of the geometry to obtain a sufficiently small critical R_m that will allow us to make a model from copper’.

5. Conclusion

We have demonstrated, with the Fury experiment, that the concept of anisotropic conductivity could be used effectively to produce a self-generated dynamo. Without any magnetic materials, just copper, and a small quantity of galinstan for electrical contact, we have built a dynamo that can be human-powered. The characteristics of the setup correspond rather well to the finite-element calculations, in terms of dynamo threshold and eigenmode of the magnetic field. When abrupt changes in the driving torque are imposed, rotation and magnetic oscillations have been put in evidence, due to the linear dynamo growth rate dependence around the threshold angular velocity.

Our measurements indicate that the magnetic field is axisymmetric. This cannot be exactly true: at small scale (smaller than the distance between the grooves), our setup is just made of materials of isotropic heterogeneous conductivity. So Cowling’s theorems apply and an axisymmetric field cannot be sustained by dynamo action. Azimuthal variations must exist but they are small and we have not measured them yet. On a meso-scale (larger than the distance between the groove and smaller than the setup), we model the configuration by a material of homogeneous anisotropic electrical conductivity. In that case, axisymmetric dynamo solutions exist. Our results prove that this modelling is adequate for Fury.

As we have seen, small scale conductivity heterogeneity can be modelled as electrical anisotropy in some cases, and this is true for our Fury experiment. However, there are other cases of electrical heterogeneity that are definitely different. For instance, a uniform flow next to a solid wall with spatial electrical conductivity modulation in the streamwise direction can lead to dynamo action [29]. In this case, the wavelength of the modulation is important and cannot be made zero. In the limit of zero wavelength, this would indeed correspond exactly to an anisotropic electrical conductivity with the flow direction as a principal axis of anisotropy. Our model of sliding plates [18] shows that such a configuration does not produce a dynamo. In another case of heterogeneity [30], an equivalent α -effect is produced but this requires velocity length-scales comparable to the length-scale over which electrical conductivity varies so that an anisotropic conductivity would not lead to the same results.

In recent years, a self-exciting dynamo with spiral arms was tested by Avalos-Zúñiga *et al.* [31]. In 2018, the dynamo threshold was reached and the results presented at the MHD days meeting in Dresden (16–28 November 2018), more results have been provided to us in a private communication (Avalos-Zúñiga RA, 2022) and a manuscript on the dynamo results is now available in ArXiv [32]. This dynamo was designed according to the concept of Bullard’s dynamo disc; however, it seems that an anisotropic conductivity would be a faithful model for this setup, too [33]. Concerning future experiments, one can imagine a hybrid solid–liquid configuration, similar to Fury but with a larger gap of liquid sodium or just a solid anisotropic rotor inside a pool of liquid sodium. The advantage of these configurations is that dynamo action would be guaranteed from the solid anisotropic part and that fluid dynamics would interact nonlinearly with the magnetic field. Considering the difficulties encountered to produce and study interesting nonlinear dynamos, this alternative might be valuable.

The name Fury was given to the setup because this is a dynamo that should have the property of a dynamo growth-rate increasing without bound above the dynamo threshold, which we called a ‘very fast’ or ‘furious’ regime [18,25]. That property is rather difficult to measure in the experiment because it would require a lot of mechanical power (within the resistance limits of the setup) to bring the rotor at a velocity well above the threshold velocity.

Data accessibility. Data and data processing files can be found at <https://mycore.core-cloud.net/index.php/s/ZuJ0zNp6JzLhVar>.

Authors' contributions. T.A.: conceptualization, data curation, formal analysis, funding acquisition, investigation, methodology, project administration, resources, software, supervision, validation, visualization, writing—original draft, writing—review and editing; F.P.: conceptualization, formal analysis, investigation, methodology, validation, writing—review and editing; M.M.: methodology, project administration, resources, software.

All authors gave final approval for publication and agreed to be held accountable for the work performed therein.

Conflict of interest declaration. We declare we have no competing interests.

Funding. We thank the Programme National de Planétologie (PNP) of CNRS/INSU, co-funded by CNES. The authors are grateful to the LABEX Lyon Institute of Origins (ANR-10-LABX-0066) Lyon for its financial support within the Plan France 2030 of the French government operated by the National Research Agency (ANR).

Acknowledgements. We wish to acknowledge the participation of students of geology in Lyon, Lucie Petit, Dana Romanoz and Paul Gomez in the measurement of the magnetic profile of the dynamo mode. Thanks are due to Andy Jackson for suggesting the name 'Fury' for the setup.

References

1. Faraday M. 1832 V. experimental researches in electricity. *Phil. Trans. R. Soc.* **122**, 125–162. (doi:10.1098/rstl.1832.0006)
2. Wilde H. 1867 Experimental researches in magnetism and electricity. *Phil. Trans. R. Soc. Lond.* **157**, 89–107. (doi:10.1098/rstl.1867.0005)
3. Staacks S, Hütz S, Heinke H, Stampfer C. 2018 Advanced tools for smartphone-based experiments: phyphox. *Phys. Educ.* **53**, 045009. (doi:10.1088/1361-6552/aac05e)
4. Bullard EC, Gellman H. 1954 Homogeneous dynamos and terrestrial magnetism. *Philos. Trans. R. Soc. Lond. A* **247**, 213–278. (doi:10.1098/rsta.1954.0018)
5. Lowes FJ, Wilkinson I. 1963 Geomagnetic dynamo: a laboratory model. *Nature* **198**, 1158–1160. (doi:10.1038/1981158a0)
6. Lowes FJ, Wilkinson I. 1968 Geomagnetic dynamo: an improved laboratory model. *Nature* **219**, 717–718. (doi:10.1038/219717a0)
7. Gailitis A *et al.* 2001 Magnetic field saturation in the Riga dynamo experiment. *Phys. Rev. Lett.* **86**, 3024–3027. (doi:10.1103/PhysRevLett.86.3024)
8. Stieglitz R, Müller U. 2001 Experimental demonstration of a homogeneous two-scale dynamo. *Phys. Fluids* **13**, 561–564. (doi:10.1063/1.1331315)
9. Monchaux R *et al.* 2007 Generation of a magnetic field by dynamo action in a turbulent flow of liquid sodium. *Phys. Rev. Lett.* **98**, 044502. (doi:10.1103/PhysRevLett.98.044502)
10. Herzenberg A. 1958 Geomagnetic dynamos, CERN theoretical study division. *Copenhagen* **250**, 543–583. (doi:10.1088/1361-6552/aac05e)
11. Ponomarenko YB. 1973 On the theory of hydromagnetic dynamos. *Zh. Prikl. Mekh. Tekh. Fiz. (USSR)* **6**, 47–51.
12. Roberts GO. 1972 Dynamo action of fluid motions with two-dimensional periodicity. *Phil. Trans. R. Soc. Lond. A* **271**, 411–454. (doi:10.1098/rsta.1972.0015)
13. Gailitis A, Lielausis O, Platacis E, Gerbeth G, Stefani F. 2003 The Riga dynamo experiment. *Surv. Geophys.* **24**, 247–267. (doi:10.1023/A:1024851818821)
14. Tilgner A, Busse FH. 2001 Saturation Mechanism in a Model of the Karlsruhe Dynamo. In *Dynamo and Dynamics, a Mathematical Challenge*. NATO Science Series, vol. 26 (eds P Chossat, D Ambruster, I Oprea). Springer, Dordrecht. (doi:10.1007/978-94-010-0788-7_13)
15. Berhanu M *et al.* 2007 Magnetic field reversals in an experimental turbulent dynamo. *Europhys. Lett.* **77**, 59001. (doi:10.1209/0295-5075/77/59001)
16. Müller U, Stieglitz R, Horanyi S. 2004 A two-scale hydromagnetic dynamo experiment. *J. Fluid Mech.* **498**, 31–71. (doi:10.1017/S0022112003006700)
17. Müller U, Stieglitz R, Busse FH. 2004 On the sensitivity of dynamo action to the system's magnetic diffusivity. *Phys. Fluids* **16**, L87–690. (doi:10.1063/1.1807451)
18. Alboussière T, Drif K, Plunian F. 2020 Dynamo action in sliding plates of anisotropic electrical conductivity. *Phys. Rev. E* **101**, 033107. (doi:10.1103/PhysRevE.101.033107)
19. Plunian F, Alboussière T. 2020 Axisymmetric dynamo action is possible with anisotropic conductivity. *Phys. Rev. Res.* **2**, 013321. (doi:10.1103/PhysRevResearch.2.013321)
20. Hecht F. 2012 New development in freefem++. *J. Numer. Math.* **20**, 251–265. (doi:10.1515/jnum-2012-0013)

21. Orlandi P, Bernardini M, Pirozzoli S. 2015 Poiseuille and Couette flows in the transitional and fully turbulent regime. *J. Fluid Mech.* **770**, 424–441. (doi:10.1017/jfm.2015.138)
22. Alboussière T, Cardin P, Debray F, La Rizza P, Masson J-P, Plunian F, Ribeiro A, Schmitt D. 2011 Experimental evidence of Alfvén wave propagation in a gallium alloy. *Phys. Fluids* **23**, 096601. (doi:10.1063/1.3633090)
23. Gillet N, Jault D, Canet E, Fournier A. 2010 Fast torsional waves and strong magnetic field within the Earth's core. *Nature* **465**, 74–77. (doi:10.1038/nature09010)
24. Tigrine Z, Nataf H-C, Schaeffer N, Cardin P, Plunian F. 2019 Torsional Alfvén waves in a dipolar magnetic field: experiments and simulations. *Geophys. J. Int.* **219**, S83–S100. (doi:10.1093/gji/ggz112)
25. Plunian F, Alboussière T. 2022 Fast and Furious dynamo action in the anisotropic dynamo. *J. Fluid Mech.* **941**, A66. (doi:10.1017/jfm.2022.349)
26. Alboussière T, Lingwood RJ. 2000 A model for the turbulent Hartmann layer. *Phys. Fluids* **12**, 1535–1543. (doi:10.1063/1.870402)
27. Petrelis F, Fauve S. 2001 Saturation of the magnetic field above the dynamo threshold. *Eur. Phys. J. B* **22**, 273–276. (doi:10.1007/s100510170103)
28. Brandenburg A, Moss D, Soward AM. 1998 New results for the Herzenberg dynamo: steady and oscillatory solutions. *Proc. R. Soc. Lond. A* **454**, 1283–1300. (doi:10.1098/rspa.1998.0207)
29. Busse FH, Wicht J. 1992 A simple dynamo caused by conductivity variations. *Geophys. Astrophys. Fluid Dyn.* **64**, 135–144. (doi:10.1080/03091929208228087)
30. Pétrélis F, Alexakis A, Gissinger C. 2016 Fluctuations of electrical conductivity: a new source for astrophysical magnetic fields. *Phys. Rev. Lett.* **116**, 161102. (doi:10.1103/PhysRevLett.116.161102)
31. Avalos-Zúñiga RA, Priede J, Bello-Morales CE. 2017 A homopolar disc dynamo experiment with liquid metal contacts. *Magnetohydrodynamics* **53**, 341–348. (doi:10.22364/mhd.53.2.13)
32. Avalos-Zúñiga R, Priede J. 2022 Realisation of Bullard's disc dynamo. ArXiv:2211.03377. (doi:10.48550/arXiv.2211.03377)
33. Priede J, Avalos-Zúñiga RA. 2013 Feasible homopolar dynamo with sliding liquid-metal contacts. *Phys. Lett. A* **377**, 2093–2096. (doi:10.1016/j.physleta.2013.06.007)